Radiation Magnetohydrodynamic Simulations of Black Hole Accretion Flows during Hard-to-Soft transitions

Taichi Igarashi (Chiba U.)

Yoshiaki Kato（RIKEN）、Hiroyuki R. Takahashi（Komazawa U.）
Ken Ohsuga（U. Tsukuba）、
Yosuke Matsumoto、Ryoji Matsumoto（Chiba U.）

Black Hole astrophysics with VLBI: Multi-Wavelength and Multi-Messenger Era @ University of Tokyo

Igarashi et al. 2020, ApJ 902, 103

Changing Look AGN

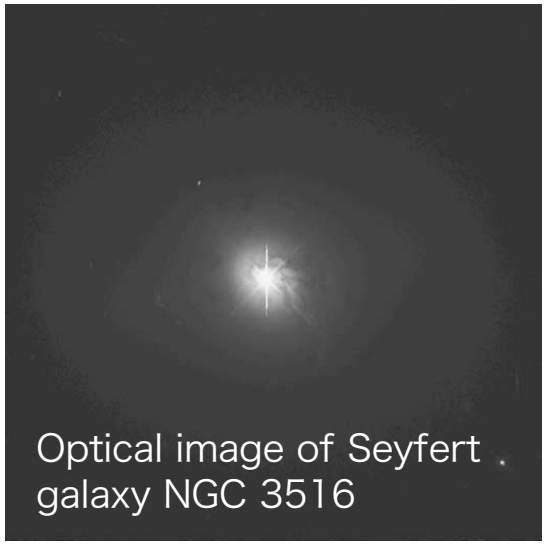
Optical image of Seyfert galaxy NGC 3516

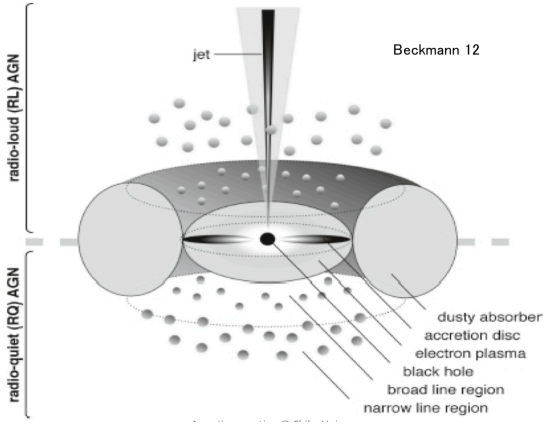

“Unified model of AGN
Beckmann 2012

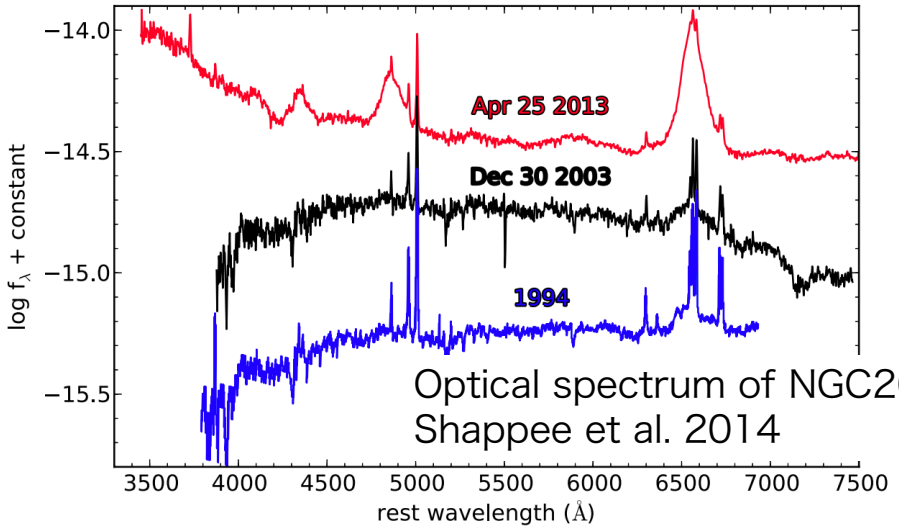

Optical spectrum of NGC2617
Shappee et al. 2014

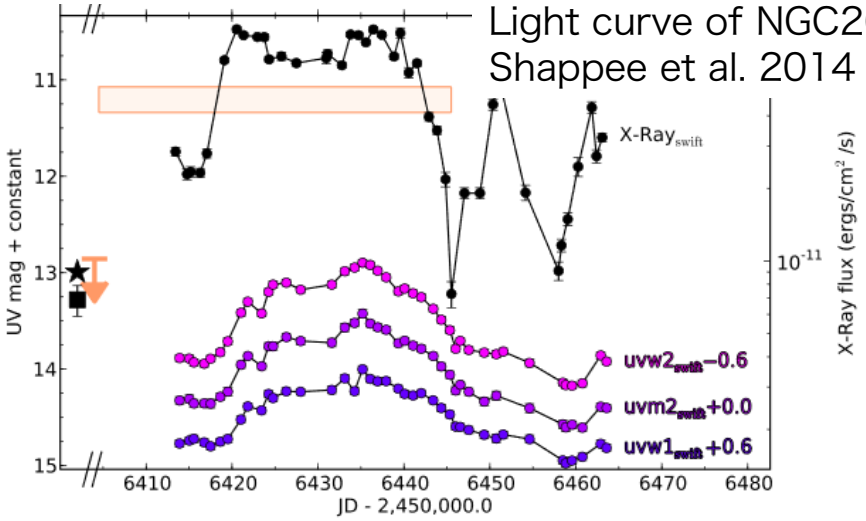

Light curve of NGC2617
Shappee et al. 2014

- CLAGN (Changing Look AGN; Shappee et al. 2014)
  - Violent luminosity variation.
  - Transit between type 1 and type 2 Seyfert galaxy.
  - Unified model of AGN cannot explain.

Spectra

Model spectrum of Mrk 1018.
Noda & Done 2018,

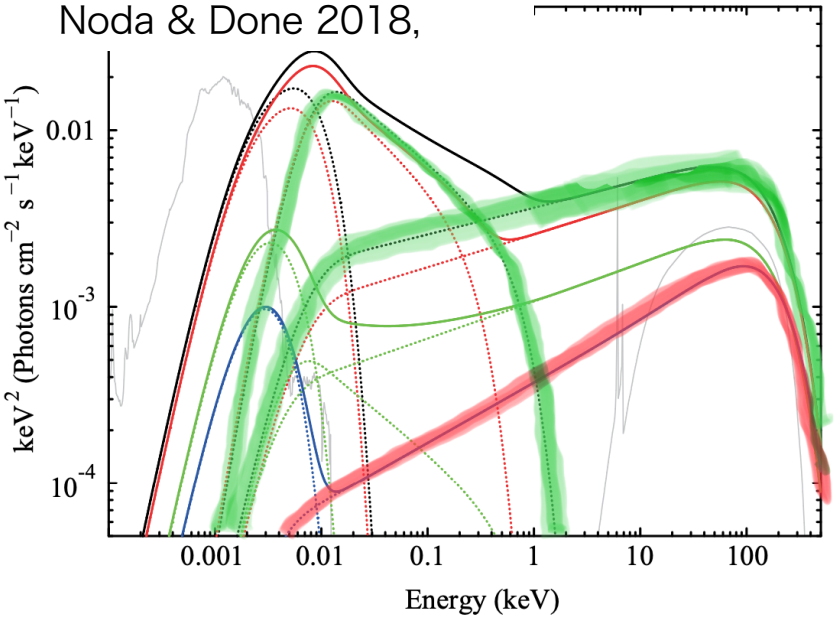

Changing Look AGNs

- Soft X-ray excess component dominant when bright state.
- Hard X-ray component dominant when dim state.

Black hole candidates show similar transition which called hard/soft, soft/hard transitions.

- Occurs during X-ray outburst.
- Violent time variation

Spectrum of Cygnus X-1
Yamada et al.2013

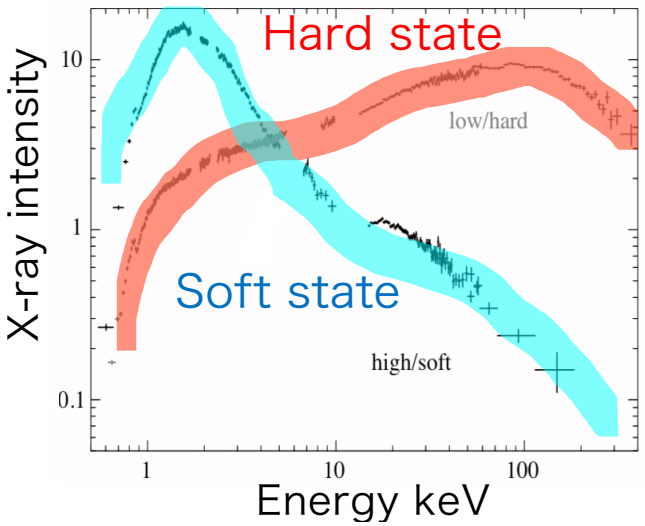

Hardness-Intensity Diagram of Black Hole Candidate MAXI J1820+070
(Shidatsu et al. 2019)

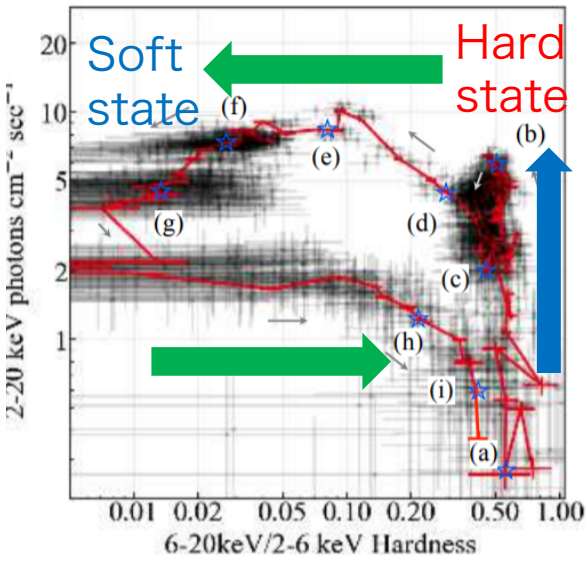

Spectra

Model spectrum of Mrk 1018.
Noda & Done 2018,

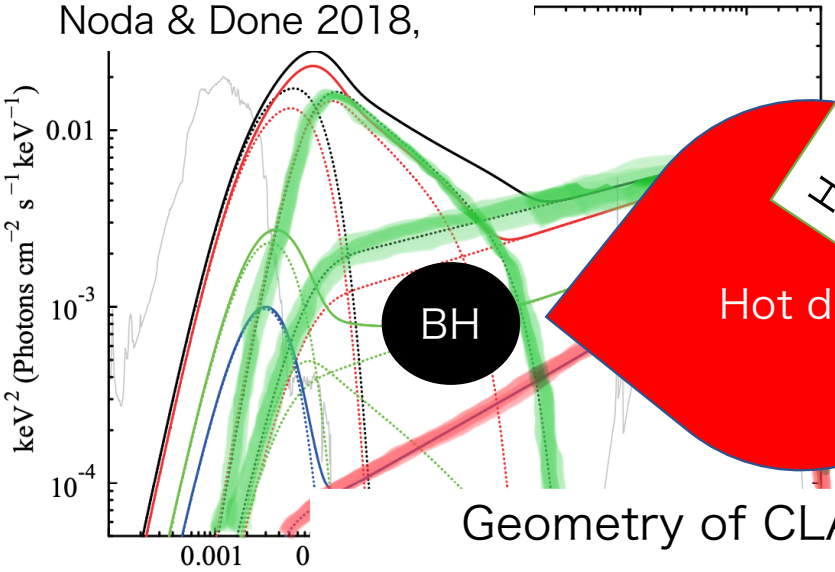

Black hole candidates show similar
ransitio ich called d/soft,
soft/h transitions
• Oc s during X- outburst.
time varia on

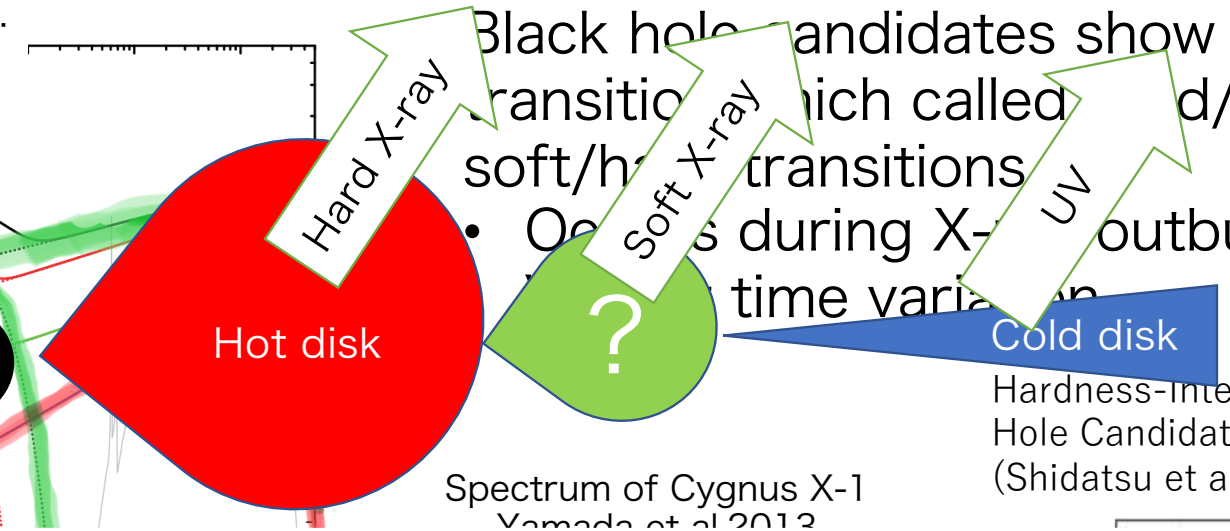

Hardness-Intensity Diagram of Black Hole Candidate MAXI J1820+070 (Shidatsu et al. 2019)

Spectrum of Cygnus X-1
Yamada et al 2013

Geometry of CLAGN (Based on Noda & Done 2018)

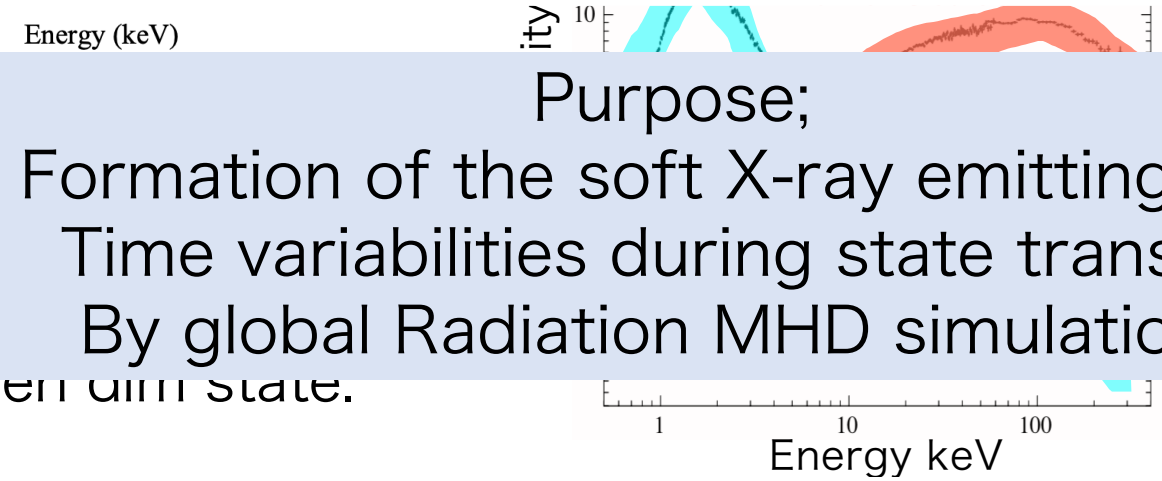

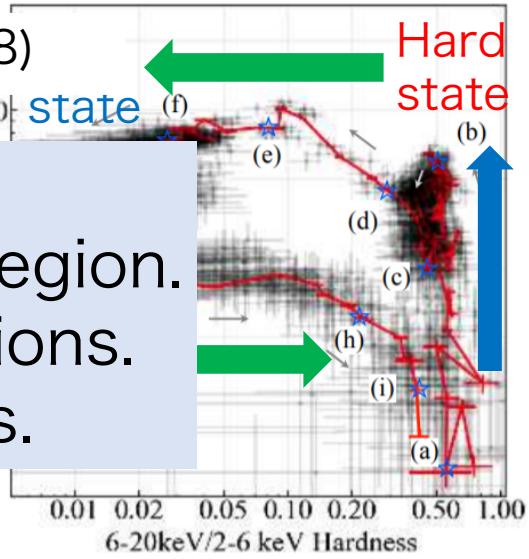

Changing Lo
- Soft X-ray
dominant
- Hard X-ra
dominant when dim state.

Purpose;
- Formation of the soft X-ray emitting region.
- Time variabilities during state transitions.

By global Radiation MHD simulations.

Basic equation

MHD

$$\frac{\partial \rho}{\partial t} + \boldsymbol{\nabla}\cdot(\rho \boldsymbol{v}) = 0$$

$$\frac{\partial \rho \boldsymbol{v}}{\partial t} + \boldsymbol{\nabla}\cdot(\rho \boldsymbol{v}\boldsymbol{v} - \boldsymbol{B}\boldsymbol{B} + P\boldsymbol{I}) = \rho \boldsymbol{\nabla}\phi_{\rm PN} - \boldsymbol{S}(\mathbb{P}_r)$$

$$\frac{\partial E}{\partial t} + \boldsymbol{\nabla}\cdot[(E+P\boldsymbol{I})\boldsymbol{v} - \boldsymbol{B}(\boldsymbol{B}\cdot\boldsymbol{v})] = -\boldsymbol{\nabla}\cdot(\eta \boldsymbol{j}\times\boldsymbol{B}) + \rho \boldsymbol{v}\cdot\nabla\phi_{\rm PN} - cS(E_{\rm r})$$

$$\frac{\partial \boldsymbol{B}}{\partial t} - \boldsymbol{\nabla}\cdot(\boldsymbol{v}\boldsymbol{B} - \boldsymbol{B}\boldsymbol{v} + \psi \boldsymbol{I}) = -\boldsymbol{\nabla}\times(\eta \boldsymbol{j})$$

$$\frac{\partial \psi}{\partial t} + c_{\rm h}^2 \boldsymbol{\nabla}\cdot\boldsymbol{B} = -\frac{c_{\rm h}^2}{c_{\rm p}^2}\psi$$

Rad. Moment eq.

$$\frac{1}{c^2}\frac{\partial \boldsymbol{F}_{\rm r}}{\partial t} + \boldsymbol{\nabla}\cdot\mathbb{P}_r = \boldsymbol{S}(\mathbb{P}_{\rm r})$$

$$\frac{\partial E_{\rm r}}{\partial t} + \boldsymbol{\nabla}\cdot\boldsymbol{F}_{\rm r} = cS(E_{\rm r})$$

Pseudo Newtonian potential

$$\phi_{\rm PN} = -\frac{GM}{R - r_s}$$

Source term

$$\boldsymbol{S}(\mathbb{P}_{\rm r}) = \rho\kappa_{\rm ff}\frac{\boldsymbol{v}}{c}(a_{\rm r}T^4 - E_{\rm r}) - \rho(\kappa_{\rm ff} + \kappa_{\rm es})\frac{1}{c}[\boldsymbol{F}_r - (\boldsymbol{v}\boldsymbol{E}_r + \boldsymbol{v}\cdot\mathbb{P}_r)]$$

$$S(E_r) = \rho\kappa_{\rm ff}(a_{\rm r}T^4 - E_r) + \rho(\kappa_{\rm ff} - \kappa_{\rm es})\frac{\boldsymbol{v}}{c}\cdot[\boldsymbol{F}_{\rm r} - (\boldsymbol{v}\boldsymbol{E}_{\rm r} + \boldsymbol{v}\cdot\mathbb{P}_{\rm r})]$$

Electron scattering opacity

$$\kappa_{\rm es} = \frac{\sigma_{\rm T}}{\rm m_p} = 0.4$$

Free-free opacity

$$\kappa_{\rm ff} = 1.7\times10^{-25}\,{\rm m_p^{-2}}\rho{\rm T_{gas}^{-3.5}}$$

MHD : CANS+(HLLD+MP5) (Matsumoto et al. 2019)

Rad : Non-relativistic version of M1-closure scheme developed by Takahashi & Ohsuga (2013)

Numerical setup

- 3D cylindrical coordinate
  - $(N_r, N_\varphi, N_z) = (592, 32, 704)$
  - $(r, \varphi, z) = ([0, 200\, r_s], [0, 2\pi], [-200\, r_s, 200 r_s])$
  - Grid size: $0.1\, r_s$ $(\mathrm{r} < 20 r_s,\ -5 r_s < \mathrm{z} < 5 r_s)$
- Units
  - length : Schwartzschild radius, $r_\mathrm{s} = 3.0 \times 10^{12}$ cm
  - velocity : speed of light, $c = 3.0 \times 10^{10}$ cm/s
  - time : $t_0 = r_\mathrm{s}/c = 100$ s
- Calculate without radiation
  - The accretion rate is constant up to $r \sim 10\, r_s$
  - Set the initial density so that $\sim 0.1 \dot{M}_\mathrm{Edd}$
  - Black hole mass $\mathrm{M_{BH}} = 10^7\, \mathrm{M}_\odot$

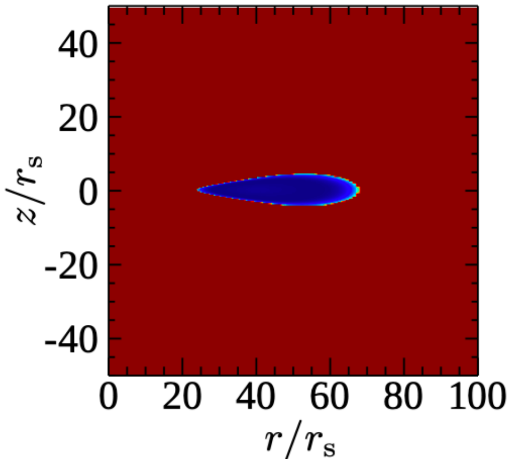

Calculate without rad. (MHD)

Absorption boundary at $2r_s$

$\mathrm{M_{BH}} = 10^7 \mathrm{M}_\odot$

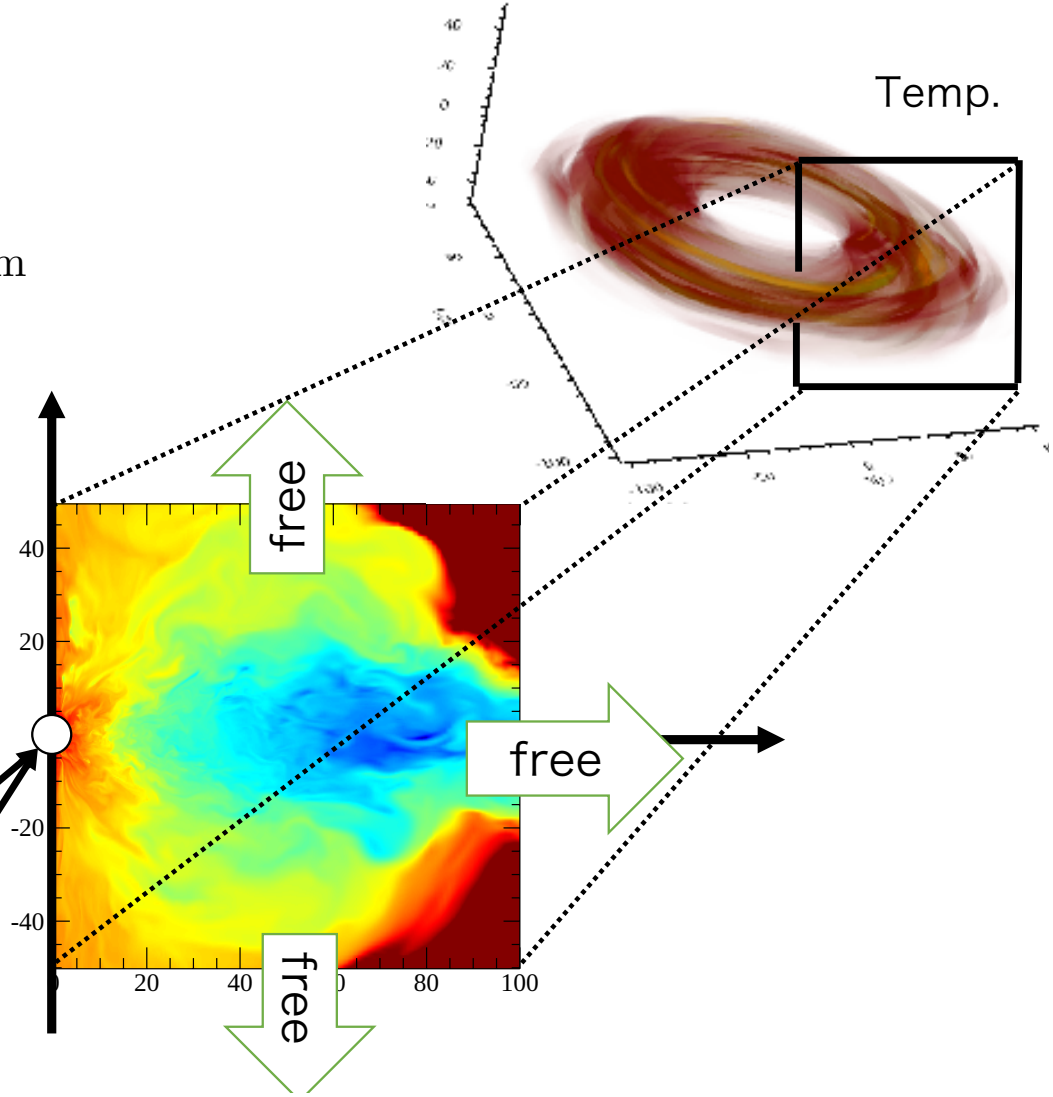

Movie of the gas temperature

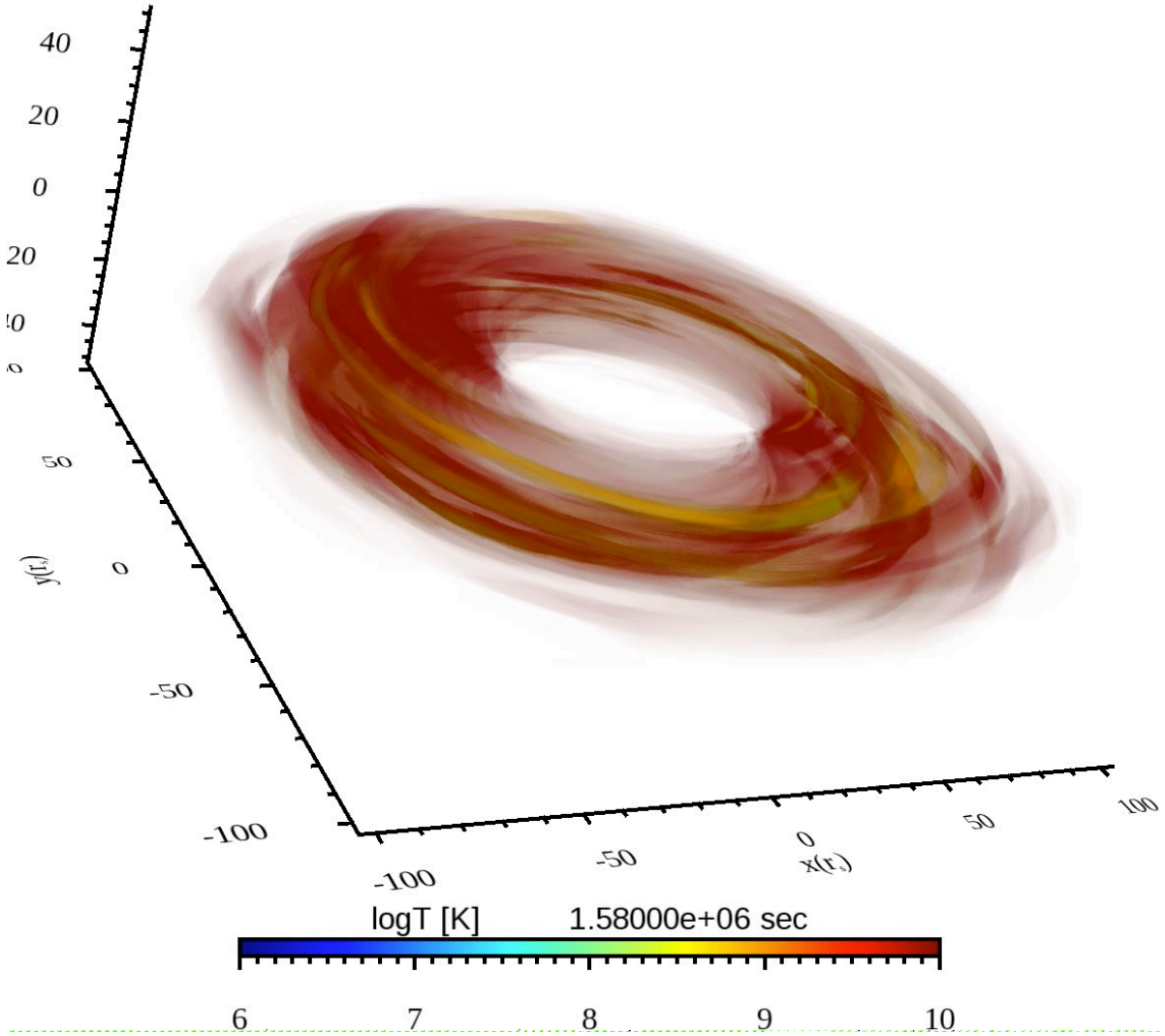

Distribution of Physical Quantities in Poloidal Plane

- Outside the hot RIAF in the inner region, cool, soft X-ray emitting region is formed in $20r_s < r < 50r_s$ by radiative cooling.
  - The disk contracts in vertical direction.

- Thomson optical depth (Contour curves in the upper panels) increases in the cool region.
  - Optically thick for Thomson optical depth.
  - But optically thin for absorption.

- Radiation energy density increase in the cool region.
  - Almost all radiation flux (Solid lines in the lower panels) is emitted from the cool region.

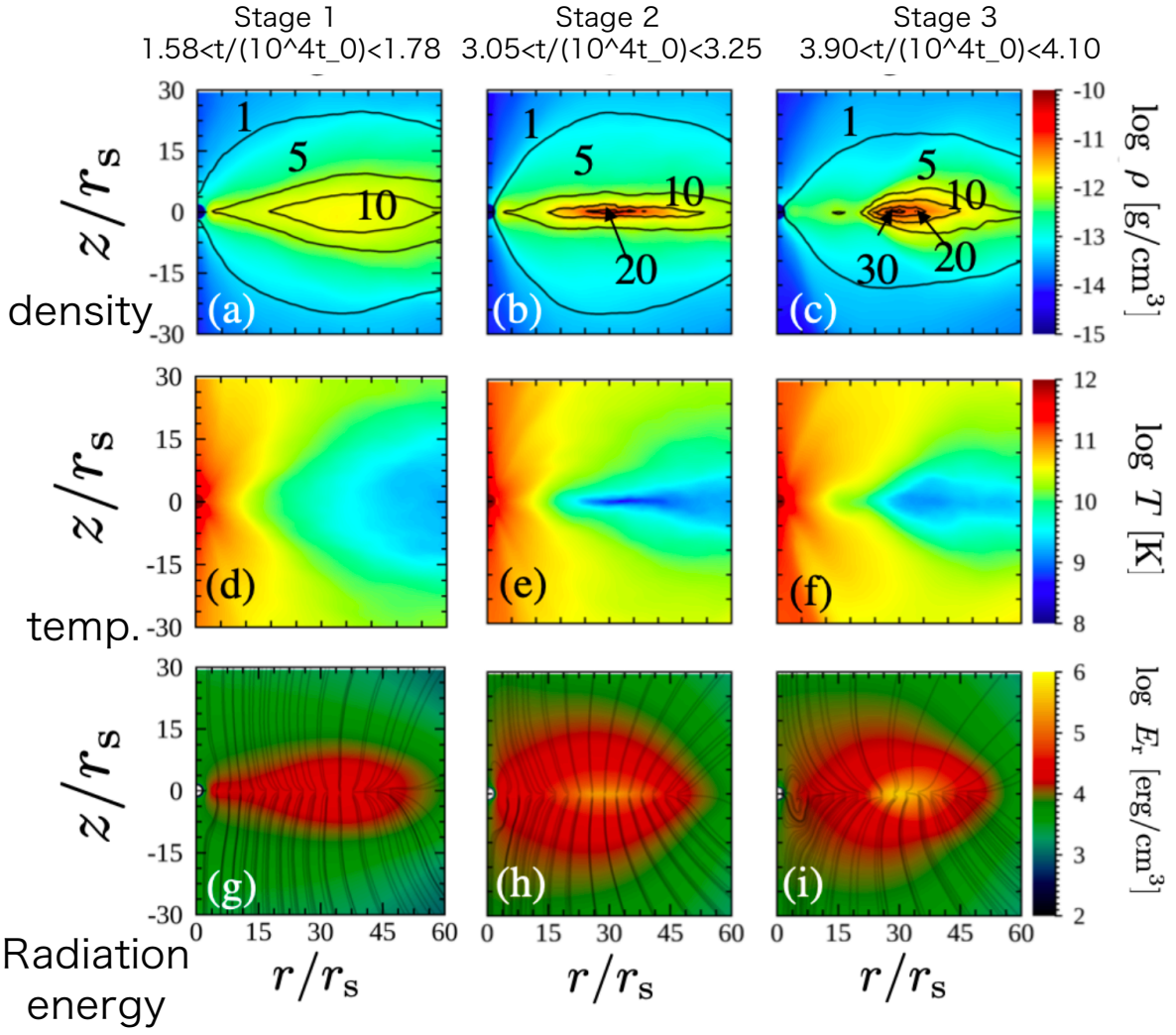

Movie of the gas temperature

- The $r - \varphi$ distribution of temperature at midplane.
- Cool region ($T < 10^8$ K) formed by cooling instability.
- Non-axisymmetric distribution of the cool region develops.
- The cool region oscillates in radial direction.

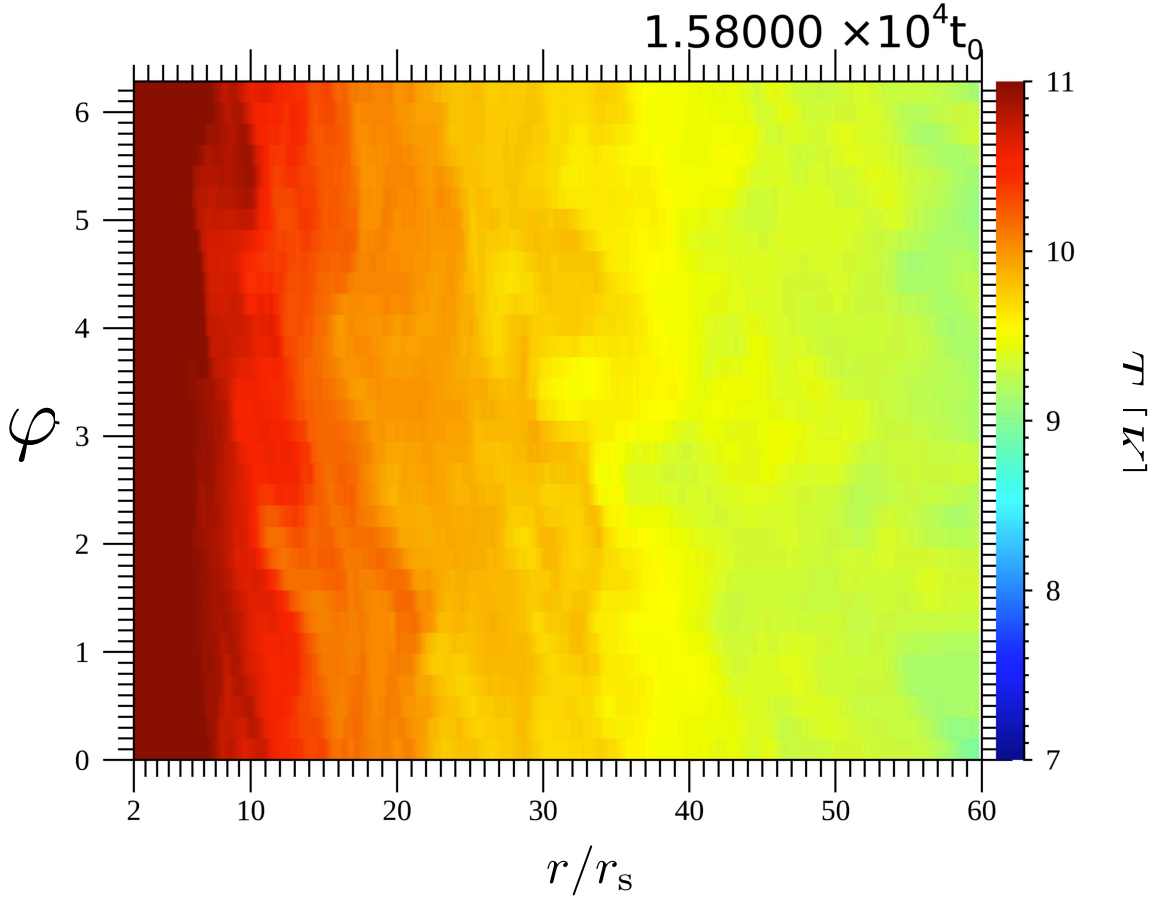

PSD

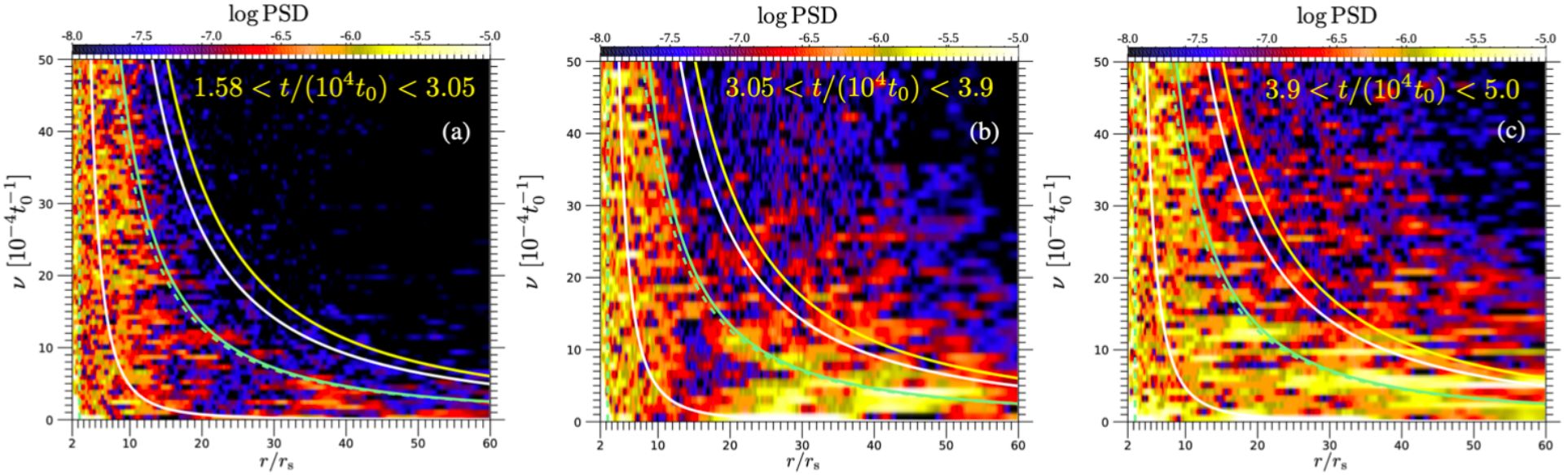

- In the early stage (a), the oscillation is localized in the hot region ($r < 20r_s$), and the frequency is below the epicyclic frequency.
- In the later stage, oscillations with frequency $\nu \sim 1\times10^{-3} t_0^{-1}$ appears around $r \sim 23r_s$.
  - The frequency correspond to Keplerian rotation frequency around r~23rs.
- In the later stage, low frequency oscillations with frequency $\nu \sim 5\times10^{-4} t_0^{-1}$ also appears is $r > 20r_s$.
  - The pulsational instability in the radiation pressure dominant region (Blumenthal et al. 1984, Kato 1978)can be responsible for this oscillation.

Green: Kepler rotation Ω_K
Dotted: epicyclic frequency κ
White: $\Omega_K \pm \kappa$
Yellow: $(1+\sqrt{2})\Omega_K$

Space-time diagram

- The $\mathrm{r}-\mathrm{t}$ distribution of the radial velocity at midplane.
- The oscillation appears around boundary between hot flow and cool region ($\mathrm{r}\sim 23r_{\mathrm{s}}=r_{\mathrm{c0}}$) at $\mathrm{t}>3\times10^{4}t_{0}$.
- The positive radial velocity indicates the over reflection of waves by corotation resonance.
- The corotation resonance (Drury 1985) can be responsible for the oscillation around $\mathrm{r}\sim 23r_{\mathrm{s}}$ ($\nu\sim1\times10^{-3}t_{0}^{-1}$).
- Another large amplitude oscillation appears $\mathrm{r}\sim 40r_{\mathrm{s}}$.

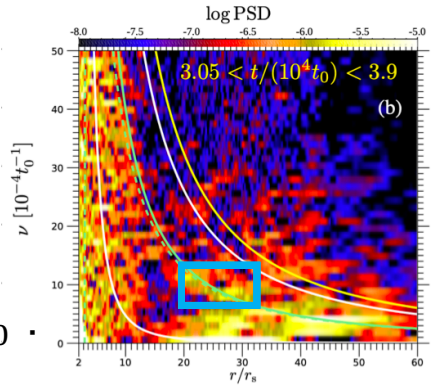

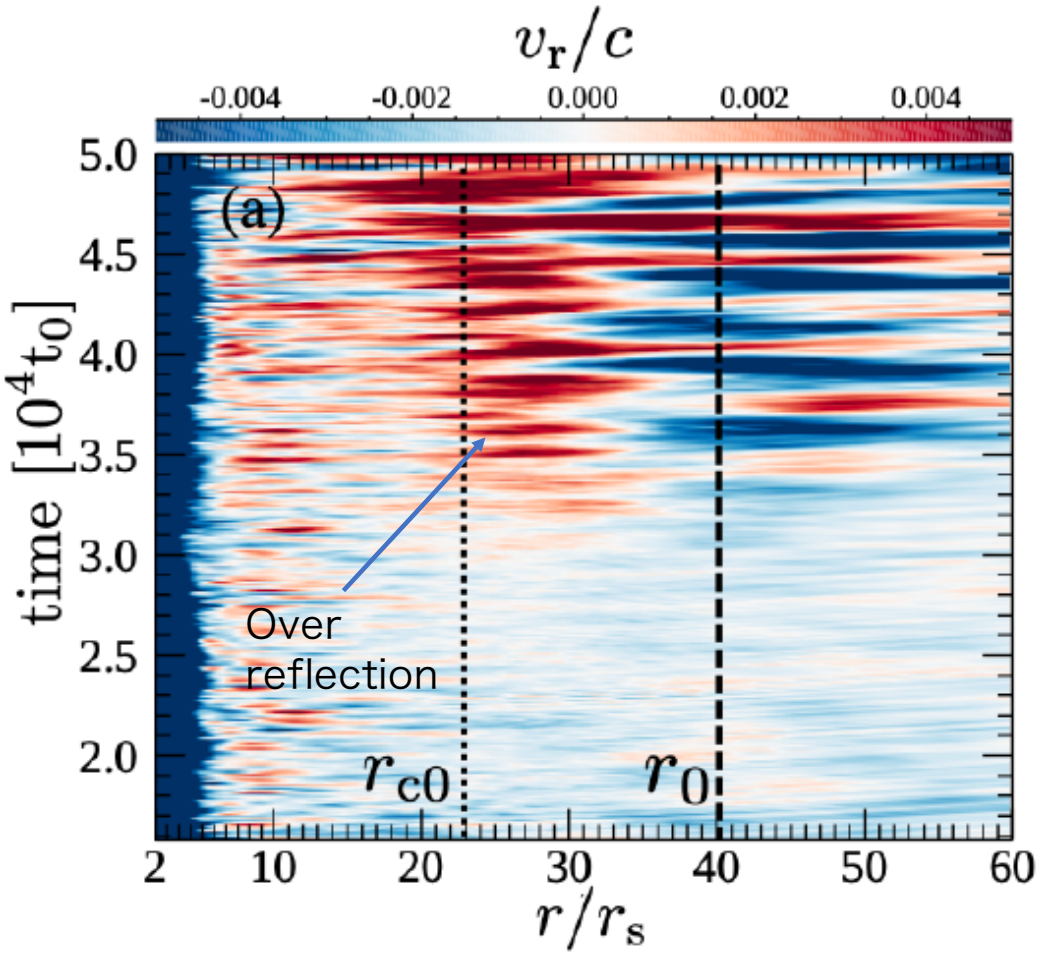

Time evolution of the cool region

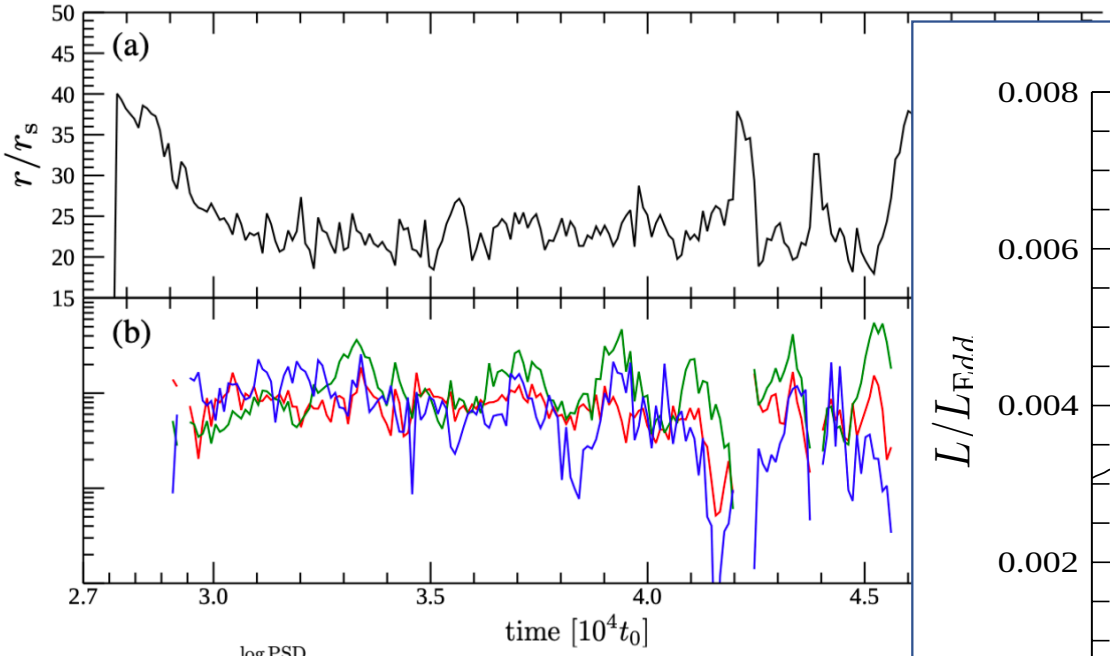

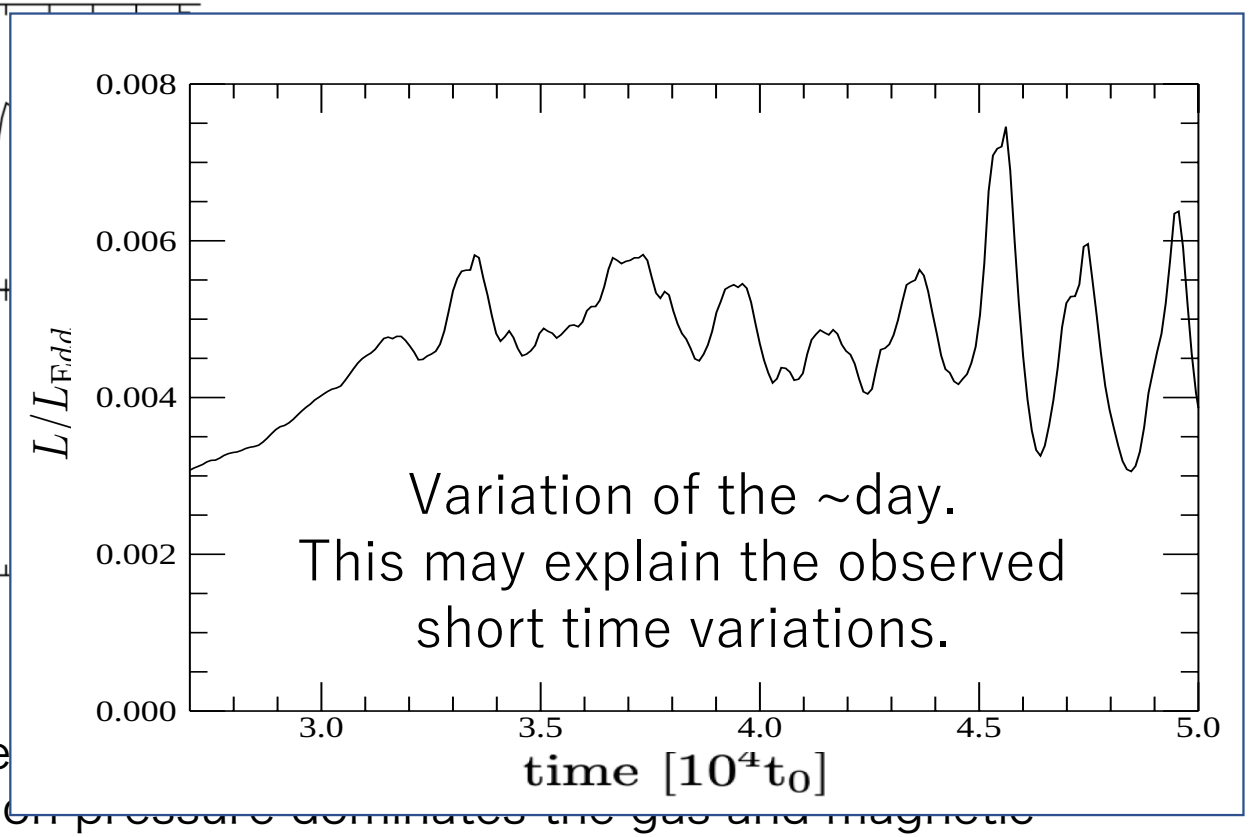

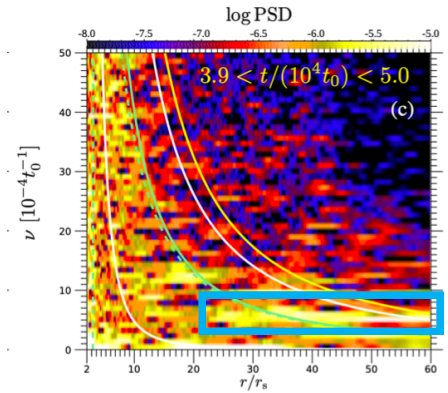

- The amplitude
  - The radiation pressure dominates the gas and magnetic pressure.
  - Amplified by the pulasational instability in the radiation pressure dominant region (Kato et al. 1978, Blumenthal et al. 1984)?

Summary

- We carried out 3D RMHD simulation of accretion flow around a supermassive black hole in CLAGNs.
- The soft X-ray emitting, cool region is formed when the accretion rate $\sim 0.1\dot{M}_{\mathrm{Edd}}$, and the region oscillates quasi-periodically.
- There are two possible mechanism of oscillations.;
  - Corotation resonance around the interface between inner hot region and cool region.
  - Pulsational instability in the radiation pressure dominant region.
- The appearance of soft X-ray emitting region and rapid time variabilities observed in CLAGNs are reproduced by RMHD simulations.